Nanostructures wetting evaluation using ultra high frequency ultrasound

Abbas Salhab, Julien Carlier, Malika Toubal, Pierre Campistron, Marc Neyens, Bertrand Nongaillard, V. Thomy

Nanostructures wetting evaluation using Ultra High frequency Ultrasound

A. Salhab [*a], J. Carlier [a], M. Toubal[a], P. Campistron[a], M. Neyens[b], B. Nongaillard[a], V. Thomy[a]

[a] Univ. Polytechnique Hauts-de-France, Univ. Lille, CNRS, Centrale Lille, UMR 8520 - IEMN-Institut d'Electronique de Microélectronique et de Nanotechnologie, F-59000

[b]STMicroelectronics, 850 rue Monnet, F-38926 Crolles, France

ABSTRACT

Ultrasounds are a great tool for defects detection particularly for optically non-transparent materials. Hence, working at very high frequency (#GHz) allows the detection of nanoscale contact defects at the interface between two materials and especially in the presence of air, which has negligible acoustic impedance, making it possible to achieve very high sensitivity.

For several years, we have been using the high frequency acoustic method for the wetting evaluation of nanostructures in our laboratory. In close collaboration with STMicroelectronics company, we deal with the study of wetting state in the context of wet cleaning processes optimization in the microelectronics industry.

Within this perspective and in order to reach these very high frequency ranges, ZnO piezoelectric transducers were developed and integrated on samples to be studied. Thanks to a dedicated workbench, the dynamic of the wetting and drying phenomena have been achieved on high-aspect-ratio nanostructures with liquid solutions having different surface tensions.

Keywords: Micro and Nano-technology, Wetting, Surface cleaning, Nondestructive testing, Acoustics, Microfluidics, Deep trench isolation, PolyDiMethylSiloxane

1. INTRODUCTION

In the year 1965, Gordon Moore published an article introducing the famous Moore's law stating that every two years the number of transistors per microchip will double in number[1]. This trend of miniaturization in the microelectronics industry led to faster integrated circuits and hence, faster computing powers. However, it is expected that down scaling transistors will reach a limit in which the transistors are unable to operate in smaller circuits due to high temperatures[2]. Thus, the semiconductor companies realized that the trend of scaling down transistors had to reach a limit someday, that's why a new trend called "More-than-Moore" introduced by the International Technology Roadmap for Semiconductors (ITRS) was adopted[3] opening the way to other developments (AI, optimization of processor architecture, neuromorphic processors, use of 2D materials or 3D integration of components). So even if the race to miniaturization will know a physical limit, the microelectronic industry will still be confronted to challenges in the fabrication at very small scales. In fact, as the sizes of the transistors reach nanometric scales, high aspect ratio (height to lateral dimension ratio) etched silicon structures are becoming increasingly common in the semiconductor industry to match the market demand for miniaturization. The fabrication of these silicon structures includes lithography processes, etching steps and multiple cleaning processes. The high aspect ratio (AR) which can reach up to 50 for these silicon structures, creates multiple issues in the industry in terms of inefficient cleaning processes[4], leading to defective microelectronic product hence, lowering the quality of the final product. The efficiency of the cleaning is linked to the different wetting conditions of the liquids used in the micro/nanometric silicon structures. When the liquid doesn't penetrates totally the etch depth of the structures, that's to say that gas pockets are located between the liquid and the solid, the wetting is only partial and the cleaning is defective. This state is known a state known as the Cassie-Baxter state[5], observed in nature for raindrop on lotus leaf[6] and often sought after for its water repellency properties but should be avoided in the case of cleaning processes of textured surfaces (Figure 1.b). When the liquid penetrates the whole etch depth of the structures, no gas pockets are present. This state is known as the Wenzel state[7] (Figure 1.a). It is not synonymous with water repellency but is necessary to achieve microstructure cleaning.

In most cases, the reality is a mixture of these two states with local combination of the two states (Cassie-Baxter and Wenzel) that could form a composite state[8](Figure 1.c).

It is commonly accepted that these wetting properties depend on both the nature of the material and the characteristics of the liquid (in particular its surface tension). Thus a flat wetting material (contact angle lower than 90°), once structured, will lead to a superhydrophilic state where the liquid drop will disappear to form a film. On the other hand, a non-wetting plane material (contact angle greater than 90°), once structured will lead to a superhydrophobic state where a drop of water will take a quasi-spherical shape. This state is called superhydrophobic and gives rise to the two Cassie-Baxter or Wenzel situations depending on the importance of the level of texturing (the more the surface will be textured, the more the Cassie-Baxter state will be favored). It is important to note that this last state is metastable and that a transition to a Wenzel state is easily generated by various factors: use of liquid with low surface tension such as oil or alcohol (technique that we will use in this paper), vibration of the surface, heating / evaporation, etc…

Another problem encountered in the semiconductor industry is the drying of the high AR silicon structures. At the micro/nanometric scales the gravitational forces are negligible and the capillary forces generated by physicochemical interactions are the dominant forces at the liquid / surface interface. Thus, after each cleaning cycle, a drying cycle is needed to dry any cleaning chemicals present in the silicon structures. During this process capillary forces play a significant role[9] in the structures deformation in a phenomenon known as "pattern collapse"[10].

A typical example of these cleaning problems due to defective wetting coupled with pattern collapse phenomena appears in the microelectronics industry. It is the case at STMicroelectronics, for one type of high AR (up to 23) silicon structures are called Deep Trench Isolation (DTI) which is generally used to isolate pixels in Complementary Metal-Oxide-Semiconductor (CMOS) image sensors[11]. This type of structure presents challenges for this company from the fact that incomplete wetting can lead to inefficient cleaning and also, in the drying cycle where the capillary forces lead to pattern collapse.

The observation and characterization of these wetting and drying phenomena at small scales and in real time is far from trivial. Many recent works of research groups have reported micro / nanoscales, high precision wetting evaluation methods[12]. One of the high resolution method used to follow the kinetics of wetting inside surface textures, is the ATR-FTIR (Attenuated Total Reflectance-FTIR)[13]. It utilizes an infrared beam sent through a crystal getting totally reflected. The analysis of the output reflected signal makes it possible to conclude on the wetting state: the penetration length of the evanescent wave in the network (around one hundred nanometers) determines the height over which the information concerning the state wetting will be obtained. At IEMN laboratory, in collaboration with STMicroelectronics, a high frequency (up to 5 GHz) acoustic method is developed[14] to characterize the wetting state of liquid droplet on micro/nanometric textured silicon wafers. While the previous work gave insights about the wetting state of some STMicroelectronics silicon structures (including DTI) using a static liquid droplet, it is far from the industrial single wafer[15] cleaning process where the cleaning liquid is dispensed dynamically.

In this work, we present the use of PolyDiMethylSiloxane (PDMS) micro-channel to create a flow of liquid on top of DTI textured silicon wafer. The use of this device leads to experimental conditions as close as possible to those used at STMicroelectronics for the cleaning processes. The micro-channel coupled with the zinc oxide (ZnO) piezoelectric transducers generating high frequency acoustic waves, will be used to characterize in real-time the dynamic wetting behavior inside the DTI structures of different etch depth (different AR).

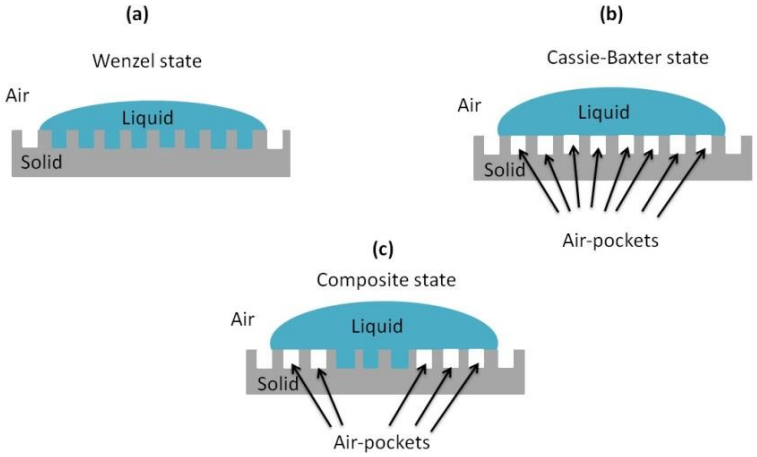

Figure 1 Schematic of different wetting states of liquid droplet that can exist on a textured surface (a) Wenzel state, (b) Cassie Baxter state and (c) Composite state

2. EXPERIMENTAL SETUP

Piezoelectric transducers

The high frequency acoustic method developed at IEMN [16] is used to characterize the wetting state of the DTI silicon wafers. The method consists of using Zinc Oxide (ZnO) based piezoelectric transducers fabricated on the back side of the DTI wafer sample (3x3 inch^2 in size). The piezoelectric transducers (100 µm circular discs) are fabricated by different layers deposition (Figure 2).

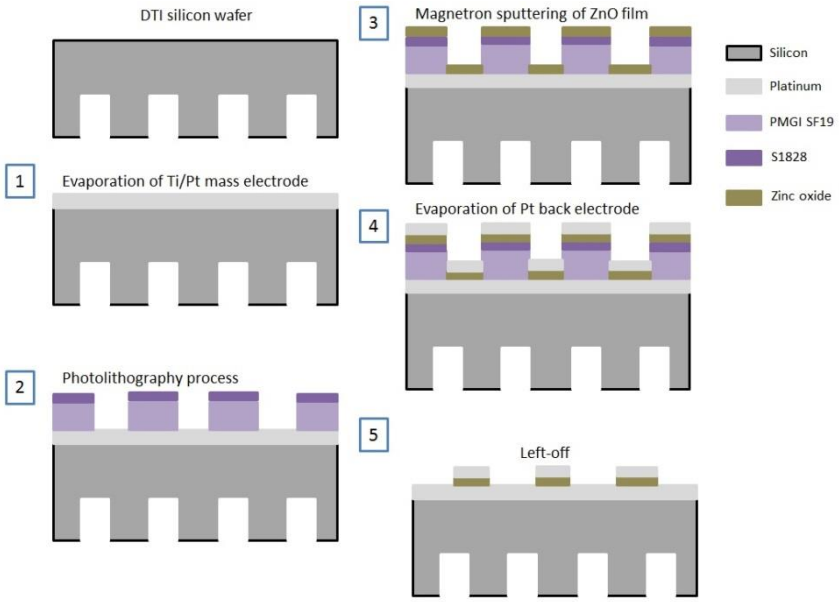

Figure 2 Schematic of the different steps included in the transducers fabrication

The fabrication process starts with 10 nm of titanium (Ti) and 50 nm of platinum (Pt) deposition by thermal evaporation on the back side of the DTI wafer. These two layers serve as a mass electrode. Then a lithography process takes place, where two resists, 8 µm layer of PMGI SF19 resist (Microchem Corporation) and a layer of 1.5µm of S1828 (Shipley Corporation) are deposited by spin coating. The resist is then exposed to Ultra-Violet (UV) light using an optical mask to define the size (100 µm) and circular shape of the transducers.

The next step includes the deposition of a ZnO piezoelectric 400 nm thin layer by Radio Frequency (R.F.) magnetron sputtering (Figure 3). The principle consists of using argon (Ar^+) ions that are attracted to the cathode before bombarding

the surface of the target (ZnO) and releasing the atoms of the material (ZnO). These latter are then deposited on the back surface of the DTI silicon wafer. The impact of the Ar^+ ions release also secondary electrons that transfer their kinetic energy to the neutral gas atoms allowing their ionization (the plasma is then self-sustained). This deposition technique is inhomogeneous in a sense that the thickness of the deposit will be slightly less at the edges than in the center of the sample. This effect causes resonant frequency variations of the transducer depending on its position on the sample. At the edges, the resonant frequency is greater (the amplitude of this variation will be more important for thinner deposited films).The ZnO sputtering process parameters are detailed in Table 1.

The last step of the fabrication process of the transducers includes the deposition of another 50 nm layer of Pt above the ZnO later. This Pt layer will take the role of a back electrode. Finally, a lift-off process is performed: the DTI sample is place in a stripper solution called SVC-14 (Kayaku advanced materials Inc.) at 70 ^{O}C with the action of magnetic agitator for about 3 hours in order to remove the deposited resist.

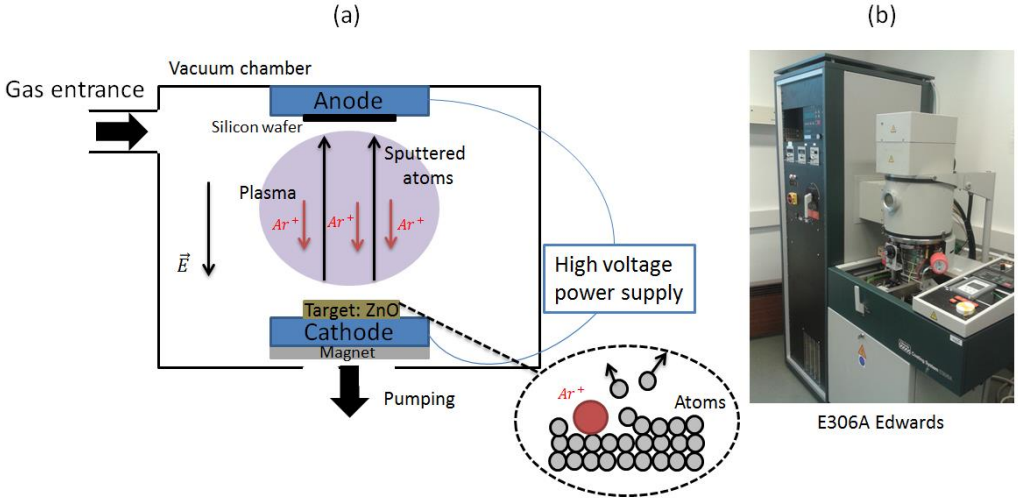

Figure 3 (a) Schematic of the magnetron sputtering process and (b) photo of the E306A Edwards magnetron sputtering equipment

Table 1 Parameters used to perform magnetron sputtering.

Power	Pressure	Flow rate ratio Argon /Oxygen	Deposition speed
120 W	0.02 mbar	8	13 nm/min

Design and fabrication of PDMS micro-channel

After fabricating the transducer on the back of the DTI wafer, the next step is to combine it with a microfluidics device to recreate liquid flow conditions as close as possible to the industrial environment. It is then necessary to design and fabricate a micro-channel. For the fabrication of this channel, the choice of a polymer molding technic (PDMS) was made for ease of implementation (both for the fabrication and for the installation of the channel on the DTI matrix). The lateral dimensions of the micro-channel are shown in Figure 4.a. These dimensions were chosen in order to completely cover the 2.1 x 2.3 mm^2 DTI matrix etched on the sample wafer (Figure 4.b). Within this array the DTI consists of periodic, etched trenches 200 nm wide (brown geometry shown in Figure 4.c). The black colored surface represents the top or smooth surface of the DTI wafer.

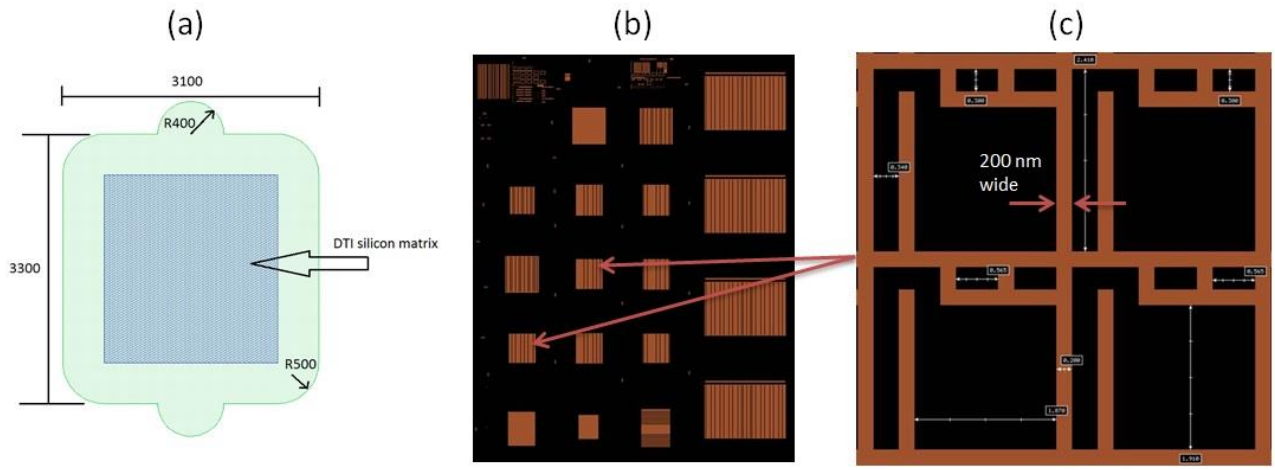

Figure 4 (a) Schematic showing the lateral dimensions of the micro-channel in µm and (b) DTI etched matrices found on the sample wafer and (c) geometry of the DTI found inside the selected matrices

In the microelectronic industry, the single wafer cleaning process is used to eliminate surface contaminants (Figure 5.a). It consists of a high pressure liquid jet, positioned on top and at a certain distance from the wafer's surface and being injected at specific flow rate on the rotating wafer. This rotation action creates a liquid film of varying thickness depending on the position from the wafer's center.

In order to reproduce the cleaning conditions (specifically the liquid flow on the surface of the wafer) used in industrial process, a PDMS micro-channel is fabricated from a molding step on a master mold. First the determination of its dimensions is calculated. The micro-channel depth is thus, deduced from data related to the liquid film thickness in the industrial cleaning process "Single wafer process" (Figure 5.b). The liquid film thickness was obtained from simulation data[17] given by STMicroelectronics which matched well the values calculated from Eq. (1)[18] for radius $|r| \geq 50$ mm using the following parameters: $Q = 0.79$ l.min^{-1}, $v = 1.10^{-6}$ m^2.s^{-1}, $w = 104.72$ rd.s^{-1}.

$$h = 0.782 \cdot Q^{0.33} \cdot v^{0.33} \cdot w^{-0.67} \cdot r^{-0.67} \quad (1)$$

Where, Q is theflow rate (m^3.s^{-1}), v the dynamic viscosity (m^2.s^{-1}), w the rotational speed (rd.s^{-1}) and r the distance from the wafer center (m).

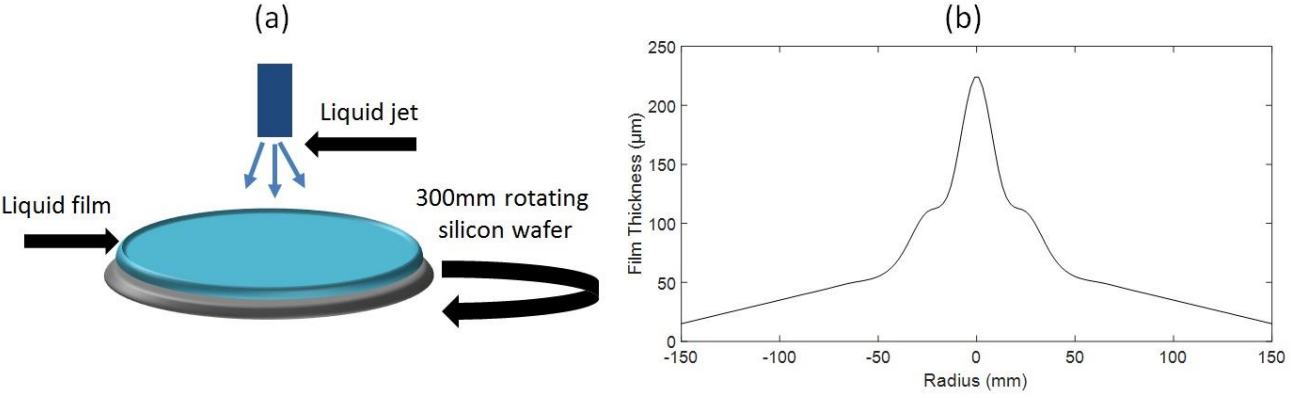

Figure 5 (a) Schematic of single wafer cleaning process used at STMicroelectronics and (b) simulation of the liquid film thickness (h) on a flat rotating silicon wafer as function of the radius from the wafer center rotating at $\omega = 1000$ r.p.m.[17]

The micro-channel depth has been taken as $2h$ to achieve the same fluid flow profile, since it is a closed channel compared to the open jet system. The radial velocity u_r of the liquid on the rotating wafer is then deduced by Eq. (2)[19].

$$u_r = \frac{w^2 r h^2 [1-(1-\frac{z}{h})^2]}{2v} \quad (2)$$

Where, z is the vertical distance from the surface of the wafer to the top of the fluid film height given as function of h (m). Integrating u_r as function of z from 0 to h and then dividing by h, we obtain Eq. (3) giving the average liquid speed u (m.s^{-1}) that will be used inside the micro-channel.

$$u = \frac{w^2 r h^2}{3v} \quad (3)$$

In order to ensure that the pressure loss inside the micro-channel doesn't exceed 1 bar which is the maximum limit of our micro-fluidic injection system, hydrodynamic calculations have been done to find out the pressure loss ΔP from inlet to outlet using Eq. (4).

$$\Delta P = \rho \cdot f \cdot \frac{L}{D} \cdot \frac{u^2}{2} \quad (4)$$

With, ΔP the pressure loss (Pa), ρ the density of the liquid (Kg.m^{-3}), L the length of the micro-channel (m), $D = \frac{2ab}{a+b}$ (a and b are the cross sectional dimensions of the micro-channel; $a = 2h$ and $b = 3.1$ mm) is the hydraulic diameter (m) and f is the friction coefficient given according to Eq. (5)[20].

$$f = \frac{64}{\mathrm{Re}} \cdot \frac{1}{\frac{2}{3} + \frac{11}{24}(\frac{b}{a})(2-\frac{b}{a})} \quad (5)$$

Where, $Re = \frac{Du}{v}$ is the Reynolds number.

Two micro-channels (depths equal to 40 µm and 80 µm respectively) were defined with the corresponding pressure loss, taking water at 20^{O}C as the liquid (Table 2). The flow rate and rotational speeds were chosen similar to conditions used at STMicroelectronics. The radius (distance from the center of the wafer) was taken so that $r \geq 50$ mm to be located away from hydraulic jump zone[21,22] (where the film thickness is drastically increased as illustrated in Figure 5.b. Also, we choose two values of the radius to study two different positions on the surface of the wafer.

Table 2 Hydrodynamic conditions for two micro-channels depths of 40 µm and 80 µm, taking water at 20^{O}C as the liquid.

~2h [µm]	**Q [L/min]**	**ν [m^2/s]**	**ω [r.p.m]**	**r [mm]**	**h [µm]**	**u_r [m/s]**	**ΔP [mbar]**
80	0.12	1.0e^{-6}	800	50	41.27	0.2	**12.56**
40	0.12	1.0e^{-6}	1000	120	19.77	0.17	**42.34**

The calculated pressure loss in the two micro-channels was in the order of tens of millibars authorizing an easy fluid actuation by our micro-fluidic pump.

After the definition of the micro-channel, a master mold (defining the shape and dimensions of the micro-channel) is made by direct laser lithography technique[23,24] using SU-8 resists (Kayaku advanced materials Inc.). The thickness of the SU-8 resist will be the same as the calculated micro-channel depth.

To fabricate the micro-channel, we used the commercial PDMS kit (Sylgard 184, Dow Coming) to make a mixture composed of 3 grams of PDMS base and 1/10 weight of curing agent. The mixture was then thoroughly mixed and exposed to vacuum to remove any air bubbles, then poured on the master mold and heated for 2 hours at 70 ^{O}C to polymerize. After that, the PDMS is separated from the master mold and using a biopsy punch with diameter equal to 2

mm, inlet and outlet are drilled. Next, the PDMS is treated by hand-held corona plasma treated (Electro-Technic Products (Chicago, IL)) for 1 minute to remove any organic material form the surface and to create silanol (SiOH) groups on the surface necessary to bond the PDMS channel to the silicon. At last, the PDMS is brought into contact to the DTI wafer making sure that the micro-channel covers the DTI matrix. Then the wafer is moved to an over for 1 hour at 70 ^{O}C to strengthen the bond between the PDMS and the wafer.

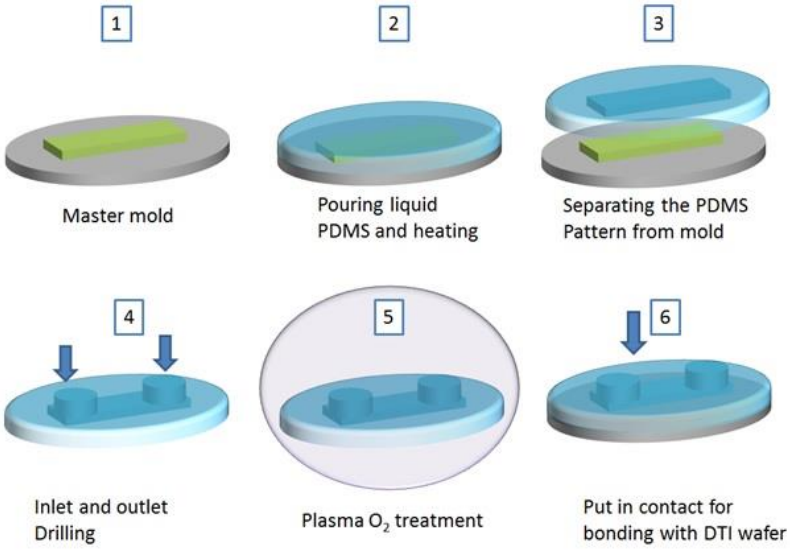

Figure 6 Schematic of the different steps involved in making a PDMS micro-channel

Micro-fluidic tubes of 0.5 mm internal diameter and of 0.8 mm wall thickness were inserted in the inlet and outlet of the micro-channel. The final system (Piezoelectric transducers, PDMS micro-channel and DTI wafer) is shown in Figure 7.

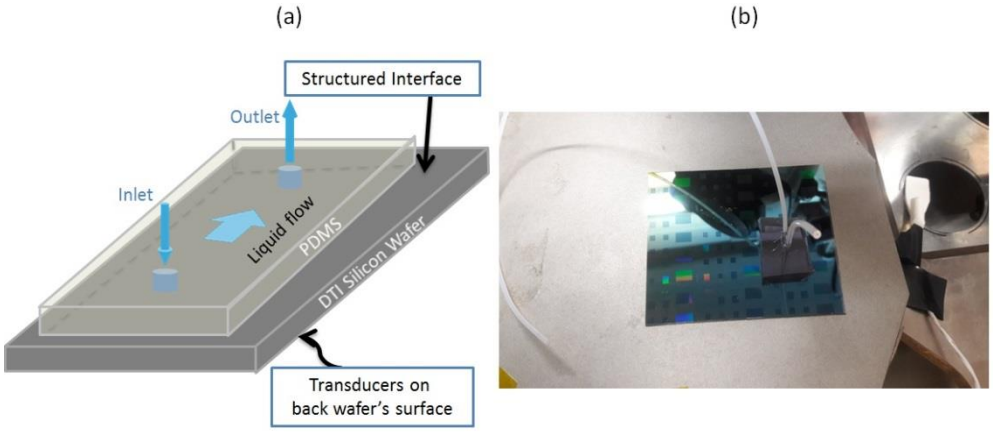

Figure 7 (a) Schematic of the DTI sample (b) image of the finished DTI sample

Measurement bench

The acoustic measurements are done on a "Backside prober" bench, where the DTI sample edges are place on a holder. Measurement point (tip) are put into contact to the transducers located on the back of the wafer. The holder has suction holes in order to prevent any movement of the sample since the contact between the tip and the transducer is highly affected by the slightest movement. The positioning of the tip on a specific transducer (100 µm in diameter) is done using a camera also found under the DTI sample. The tip is connected to a Victor Network Analyzer (VNA) in order to electrically excite the piezoelectric transducer. The transducer function is then two folds: to emit acoustic waves and receive the electrical signal of the reflected acoustic signals.
We used ZVA 8 ROHDE & SCHWARTZ" VNA which has a frequency band up to 8 GHz. A micro-fluidic system

MFCS-FLEX (from Fluigent company) was used to control the fluid flow inside the micro-channel by variation of pressure up to 1 bar. The liquid is injected into the micro-channel during the wetting phase at pressure of 300 mbar and flow rate varying between 4 $ml.h^{-1}$ and 5 $ml.h^{-1}$. During the drying phase ambient air is injected into the micro-channel at a pressure of 1bar. Another fluidic pump (Agilia syringe pump, Fresenius Kabi AG) is used to achieve higher flow rates in order to reach the calculated liquid velocity in the micro-channel (Table 2). It is capable of injecting liquid into the micro-channel at flow rates varying from 100 $\mu l.h^{-1}$ up to 120 $ml.h^{-1}$. The Agilia syringe pump was used since, the previous flow rate used in the Fluigent pump (between 4 $ml.h^{-1}$ and 5 $ml.h^{-1}$) does not allow us to reach the calculated liquid velocity (Table 2). The micro-channel inlet was connected to each pump by a microfluidic tube of internal diameter equal to 0.5 mm. The measurement bench is presented in Figure 8.

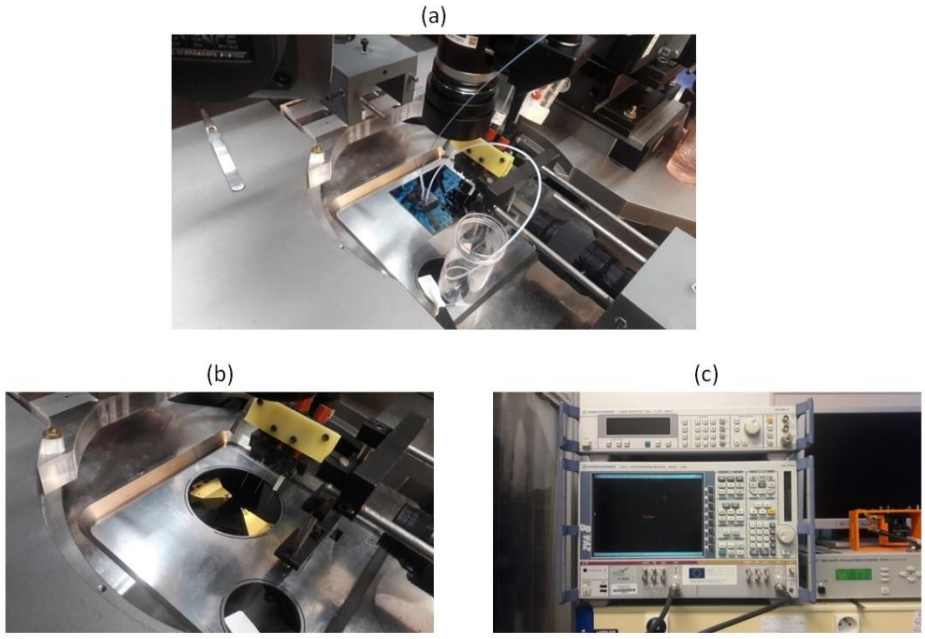

Figure 8 Images of the measurement bench showing (a) DTI sample wafer placed on holder and connected to the microfluidic system, (b) measurement tips located under the holder and (c) VNA connected to the tips

Measurement protocol

After setting up the DTI sample on the measurement bench, the amplitude of the reflected acoustic signal is displayed from the echoes diagram $S_{11}(t)$ in the time domain. A MATLAB program allows the acquisition of the amplitude of the reflection coefficients (r_1 and r_2), as function of time, on the top and bottom surface of the DTI respectively. The formulas for calculating r_1 and r_2 are given in Eq. (6).

$$|r_1| = \frac{A_{11}^{liquid}}{A_{11}^{air}}; |r_2| = \frac{A_{12}^{liquid}}{A_{12}^{air}} \quad (6)$$

With A_{11} and A_{12} are the amplitudes of the reflected wave (echo) of the bottom and the top surface of the DTI respectively (Figure 9).

In the presence of a liquid, the acoustic energy gets absorbed and the amplitude of the reflected signal decreases. Thus, r_1 and r_2 have value comprise between 0 and 1 ($0 < r_1 \leq 1$ and $0 < r_2 \leq 1$).

We are mainly interested in the value of r_1 to determine the wetting state inside the DTI. After obtaining the value of r_1 for a certain liquid, it is compare to a measured value on smooth silicon wafer in the presence of the same liquid (state of total wetting). Then, depending on the value obtained on the DTI sample, conclusions are made about the wetting state. For example, in the presence of water, $r_{1/water}$ = 0.86 in the state of complete wetting (liquid deposited on a smooth

silicon surface) and $r_{1/ethanol}$ = 0.91 for complete wetting in the presence of pure ethanol on a silicon surface. In the presence of air, the acoustic energy is not absorbed so, $r_{1/air}$ = 1.

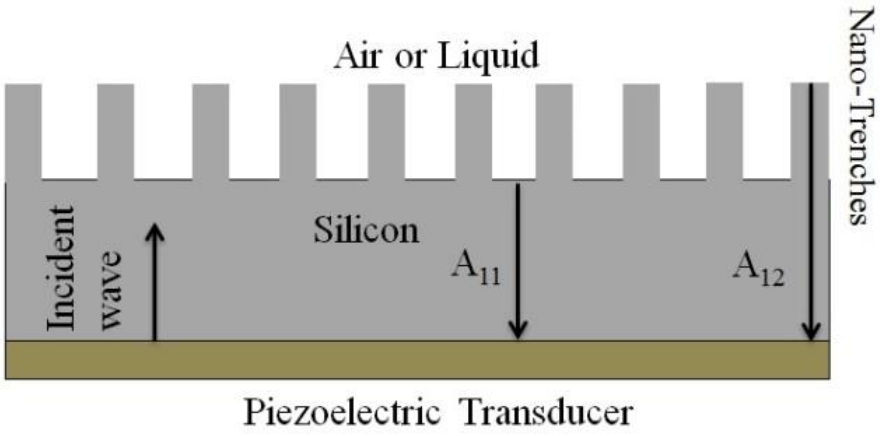

Figure 9 Schematic of the incident wave and the reflected acoustic signals (A_{11} and A_{12}) on a textured surface.

3. RESULTS AND DISCUSSION

In what follows we will present the measurements of the acoustic reflection coefficients (r_1 and r_2) for DTI wafers of different etch depths (4, 5, 6 and 7 μm) using Distilled Water (DW) and ethanol solutions at different concentrations so that to study the wetting transition by gradually varying the surface tension of the liquid, at room temperature. The ethanol and water were chosen since they are linked to the two extreme values of the surface tension (22.31 mN.m-1 and 72.75 mN.m-1 respectively[25]). Piezoelectric transducers of diameter 100 μm generate longitudinal waves of central frequency between 3.5 GHz and 4 GHz. on the VNA, the spectral band was fixed between [1 GHz - 6 GHz] while the number of sweep points was set to 10000 and the resolution bandwidth to 10 KHz. First we will introduce the measurements with the 40 μm deep micro-channel using different ethanol / Distilled Water (DW) mixtures. The liquids will be injected in the micro-channel at a pressure of 300 mbar and for the drying process ambient air will be injected at a pressure of 1 bar. Then we will introduce the developed automated data acquisition system using the 80 μm deep micro-channel. By this automation, the acquisition time between two consecutive data measurements was no more than 12 sec, which constitutes a very substantial improvement, compared to 1 -2 minutes for the static measurements used in the case of 40 μm deep micro-channel. This feature is particularly important to study drying phenomena that can take place over very short periods of time. This new technique will also increase the precision on the obtained values of the reflection coefficients from Δr_1 = 0.05 to Δr_1 = 0.0025.

Micro-channel 40 μm deep: Static data acquisition

The results presented here refer to DW / ethanol injected inside the 40 μm deep micro-channel at room temperature. Between each liquid measurement the air is injected until the DTI network is completely dry which results in a reflection coefficient corresponding to air (r_1 = 1). The calculation of the reflection coefficient for each liquid injection was done directly using the echoes diagram obtained from the VNA. The reflection coefficients r_1 as function of ethanol volume concentration, at room temperature, for the DTI 4, 5, 6 and 7 μm are shown in Figure 10.

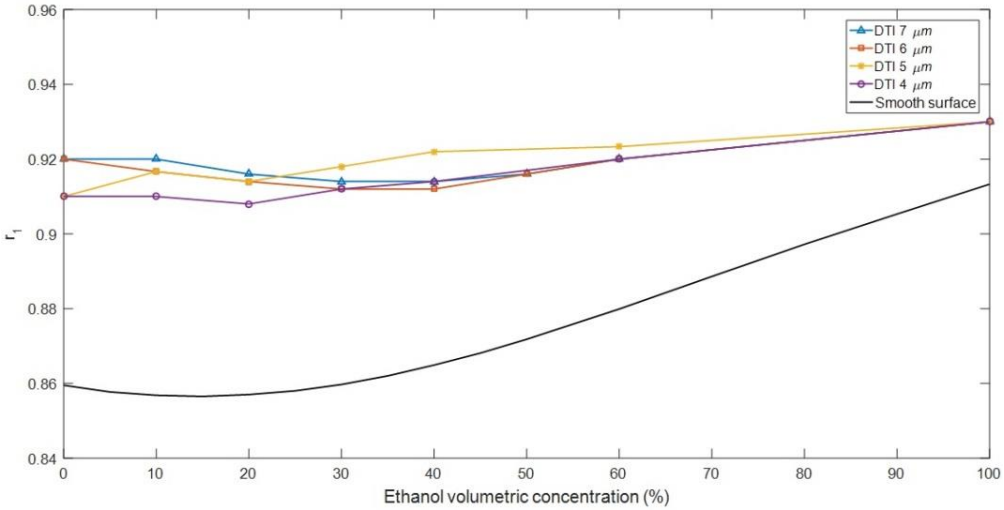

Figure 10 Variations of the reflection coefficient r_1 on the bottom of the DTI 4, 5, 6 and 7 µm for different DW / ethanol mixtures using 40 µm deep micro-channel.

We can observe, from the obtained values for the DTI network, that r_1 values are always superior to those obtained for silicon smooth surface. For example, in the case of water and pure ethanol for the DTI 4 µm we obtained values of 0.91 and 0.93 respectively which are significantly higher than the values obtained on smooth surface (0.86 and 0.91). These overestimations indicate that wetting inside the trenches is not total and could be related to air being trapped in the network. Thus, the amount of reflected energy will be greater than that in a purely Wenzel state, implying an increase in the reflection coefficient and non-complete wetting inside the trenches.
Approximately the same wetting response is observed on the four DTI samples despite the aspect ratio difference of the trenches ranging from 20 for the 4 µm DTI up to 35 for the 7 µm DTI sample.

Wetted surface: 40 µm deep micro-channel

It was concluded, from the comparison of the reflection coefficients (r_1) measured on the different DTI samples with the theoretical reflection coefficient obtained on a silicon (Si) smooth surface ($r_{Si/liquid}$), that partial wetting state is obtained with the use of different water / ethanol mixtures. Two scenarios are then possible in the case of partial wetting. The first one consider a uniform wetting on all the etched trenches but with trapped air pockets and a changing meniscus depending on the contact angle (Figure 11.a and Figure 11.b). In the second scenario we have a composite wetting state where some trenches are completely filled with liquid and others are filled with air (Figure 11.c). In either case, it is possible to calculate the unit area fraction of wetted surface S_w using Eq. (7).

$$r_1 = S_w \cdot r_{Si/liquid} + (1 - S_w) \cdot r_{Si/air} \tag{7}$$

Knowing that $r_{Si/air} = 1$, we can calculate S_w using Eq. (8).

$$S_w = \frac{1 - r_1}{1 - r_{Si/liquid}} \tag{8}$$

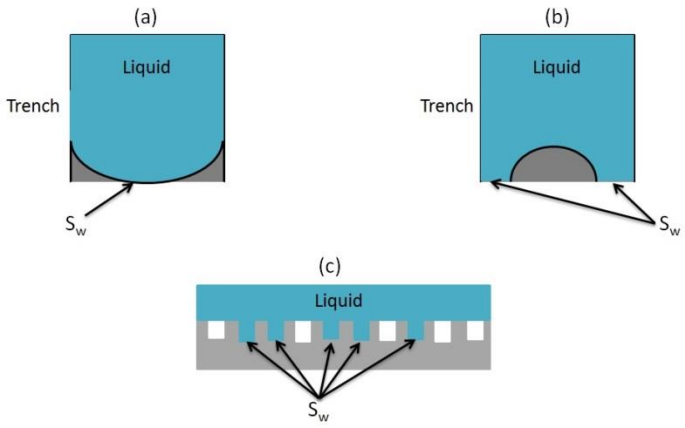

Figure 11 Schematic of possible cases behind partial wetting (a) for non-wettable hydrophobic trench surface with trapped air pockets, (b) wettable hydrophilic trench surface with trapped air pockets and (c) composite state with some trenches filled with liquids

Using the calculated reflection coefficients r_1 for the different ethanol / water mixtures, the percentage of wetted surface (% S_w) is plotted against the percentage of ethanol volume concentration (% Eth) for the four DTI samples (Figure 12).

We can observe that the general trend on all the four DTI samples was an increase in the surface area as the ethanol concentration increases, starting from about 60 % wetted area for water up to 80 % wetted area for pure ethanol.

While S_w can give general idea about partial wetting state, it was difficult to differentiate the percentages of wetted surface of the different ethanol / water mixtures since the percentage error on S_w was dependent on the ethanol concentration as shown in Eq. (9).

$$Error = \frac{\Delta S_w}{S_w} = \frac{\Delta r_1}{1 - r_1} \tag{9}$$

Here Δr_1 was obtained from multiple data measurements and taken as 0.005.

The percentage error ranged from 6 % for water, up to 9 % for pure ethanol as we can observe using the error bars on Figure 12.

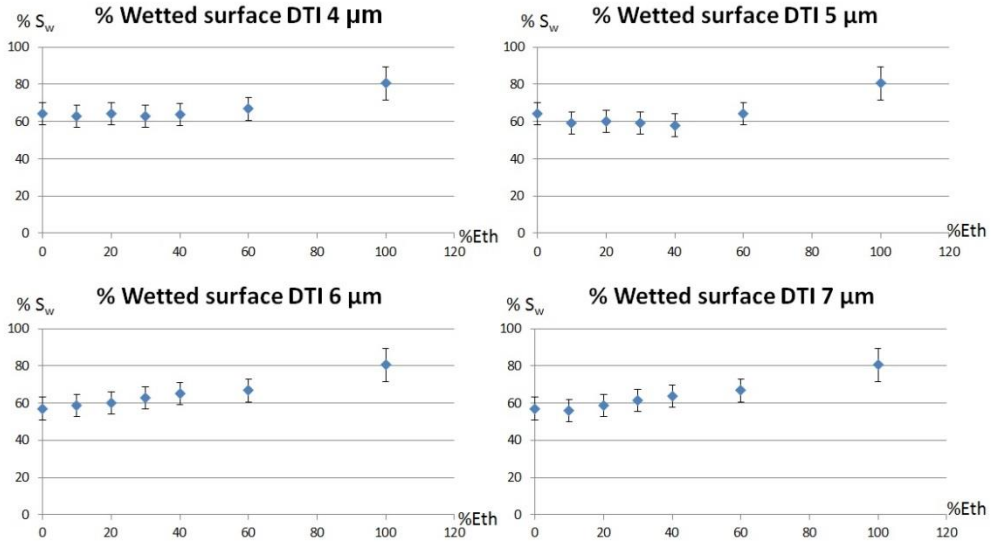

Figure 12 Percentage of wetted surface (% S_w) for different ethanol / DW concentration on the DTI samples with 40 µm deep micro-channels

Micro-channel 80 µm deep: Automatic data acquisition

For the previous results concerning the 40 µm deep micro-channel we have calculated the reflection coefficient directly from the echoes diagram by taking into account the ratio of the bottom surface DTI amplitudes when the PDMS micro-channel is filled with liquid and when it is filled with air. We also notice that the precision and stability of the reflection coefficient increases when we have higher amplitude of the reflected echoes. The amplitude on the DTI silicon interface was low (1-2 mV) because of the acoustic diffusion compared to the smooth silicon surface (15-20 mV). To make the measurements more stable, we used two measurement points, one on the DTI matrix and the other on a smooth surface. Then we normalized the reflected signals taken on the DTI surface by the amplitude of the signal taken on the smooth surface. Using this technique, the measurements of the acoustic reflection coefficient were more stable and a precision of $\Delta r_1 = 0.0025$ was achieved.

To make the data acquisition process more efficient, we developed a MatLab program to calculate the acoustic reflection coefficient as a function of time. This program takes the values of the echo's amplitudes directly from the VNA and calculates the acoustic reflection coefficient on the bottom (r_1) and top (r_2) surface of the trenches. This technique decreased the data acquisition time between two consecutive measurements to 12 sec and will be used for the measurements presented in the rest of this paper.

The measurements of the acoustic reflection coefficient r_1 using water/ethanol mixtures injected in the 80 µm deep micro-channel are shown in Figure 13.
By observing the different curves for the DTI samples, we can notice a similar response to the measurements obtained with the 40 µm micro-channel. All the obtained values for r_1 are superior to the ones obtained on a smooth surface suggesting the same conclusion mentioned for the 40 µm micro-channel with partial wetting on the bottom of the trenches.

The variations of r_1 for the same trench depth between the two micro-channels are in the range of ± 0.01. This shows that the change of the liquid film thickness "2*h*" from 40 µm to 80 µm has little significance on the wetting state.

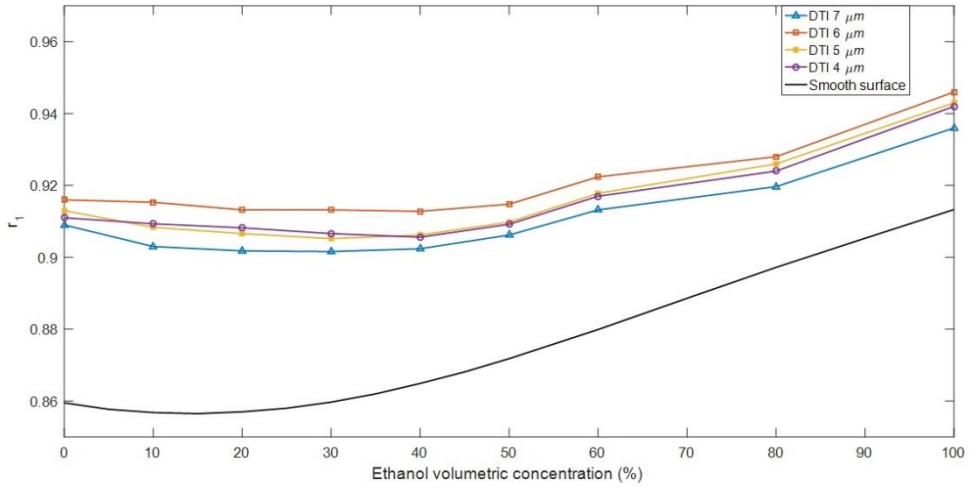

Figure 13 Variations of the reflection coefficient r1 on the bottom of the DTI 4, 5, 6 and 7 µm for different DW / ethanol mixtures using 80 µm deep micro-channel.

Wetted surface: 80 µm deep micro-channel

The percentage of wetted surface % S_w is plotted against the ethanol volume concentration (% Eth) for the DTI samples with 80 µm micro-channel (Figure 14).

As in the case of 40 µm micro-channel,the percentage of wetted surface, % S_w ranged from 60 % for water up to 80 % with the increasing ethanol concentration. The precision of the measurement on the reflection coefficient is improved with the introduction of the real-time measurements technique which in turn reduced the percentage error on S_w. The percentage error ranged from for 3% for water up to 5 % for pure ethanol as illustrated using the error bars. However, the percentage error was still too high to differentiate the wetted surface between the different ethanol concentrations.

The general trend of the plot for all the DTI samples was an increase in the wetted surface as the ethanol concentration increases in the mixture except for the points corresponding for 80 % ethanol and the pure (100%) ethanol for which we can observe a decrease that was surprising.
Considering the scientific literature about solubility of nitrogen and oxygen, the main constituents of air (21% oxygen and 78% nitrogen) in water or ethanol, it is found to be higher in ethanol than in water[26,27,28] for both gases. Thus, the diffusion of air in the pure ethanol should be higher than the 80% ethanol / water mixture. It means that we should expect a higher wetted surface for pure ethanol than for mixtures which contain water.

Therefore, up to now, a possible explanation would be that this decrease is due to the error rate on S_w valued 4 % for 80% ethanol concentration and 5 % for pure ethanol. All errors here calculated for $\Delta r_1 = 0.0025$.

In order to get a precise measurement of the wetted surface, higher precision on the value of the reflection coefficient r_1 is needed that would require higher amplitude of the reflected acoustic signal. This higher amplitude was difficult to achieve due to the diffusion (energy loss) of the acoustic waves in the DTI network. Nevertheless, it makes it possible to have a quantitative evaluation of the wetting state.

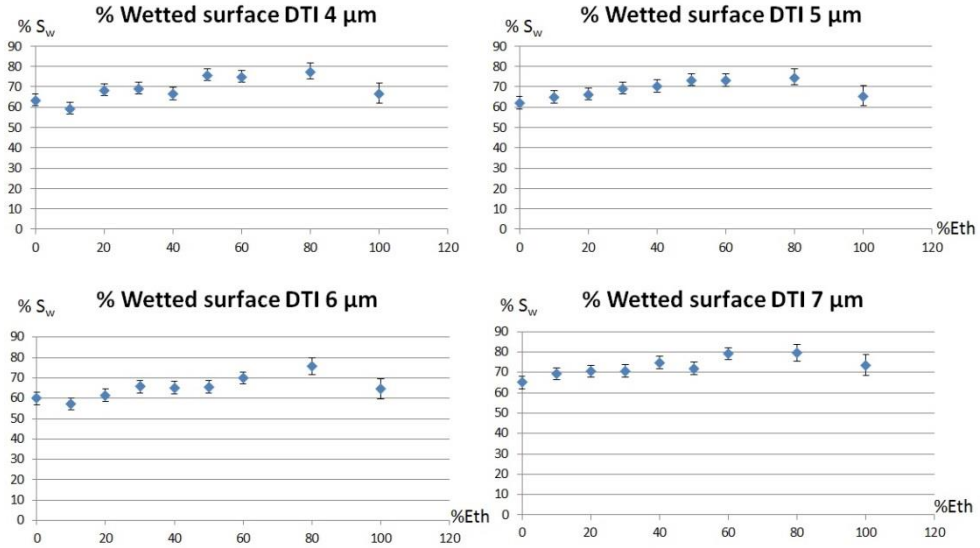

Figure 14 Percentage of wetted surface (% S_w) for different ethanol / DW concentration on the DTI samples with 80 µm deep micro-channels

Flow rate effect on wetting state

The effect of changing the flow rate with time was studied using two different liquids, distilled water and ethanol respectively. The sample was chosen to be the DTI 4 µm with micro-channel of 80 µm thickness. The DTI 4 µm was chosen because it presents the lowest aspect ratio (20) which is the ratio of the trenches depth (4 µm) to the trenches width (200 nm). If any changing on the wetting state occurs it will be easier to observe it on the lowest aspect ratio structures.

The measurements with ethanol on the DTI 4 µm are shown in Figure 15. At different time delays the flow rate was changed represented by the arrows. At t = 280 sec ethanol reaches the micro-channel with a flow rate of 10 ml.hr^{-1}, r_1 decreases from 1 to a value of 0.94 which was previously obtained for the DTI 4 µm (Figure 13). After this transition, r1 stays stable throughout the flow rate changing from 10 ml.h^{-1} up to 120 ml.h^{-1}. Calculating the fluid speed (u) at flow rate (Q) equal 120 ml.hr^{-1} taking 0.5 mm (D) as the internal diameter of the tube, we get $u = 0.17$ m.s^{-1}.

We note that this fluid speed is very close to the one calculated (Table 2) and used at STMicroelectronics cleaning system for 80 µm height micro-channel (0.2 m.s^{-1}). The use of flow rate above 120 ml.h^{-1} was not possible due to the pump characteristics (beyond the maximum flow rate). These results show that there is no wetting transition occurring with the flow rate changing in case of ethanol.

The same measurement with DW on the DTI 4 µm is shown in Figure 16. At different time delays the flow rate was changed (represent by arrows). At t = 350 sec water reaches the micro-channel with a flow rate of 10 ml.hr^{-1}, r_1 decreases

from 1 to a value of 0.92 which was slightly higher than 0.91 obtained for the DTI 4 µm (Figure 13). After this transition, r_1 stays stable throughout the flow rate changing from 10 ml.h^{-1} up to 120 ml.h^{-1}. Here again the same response is obtained with DW: there is no wetting transition occurring with the flow rate changing.

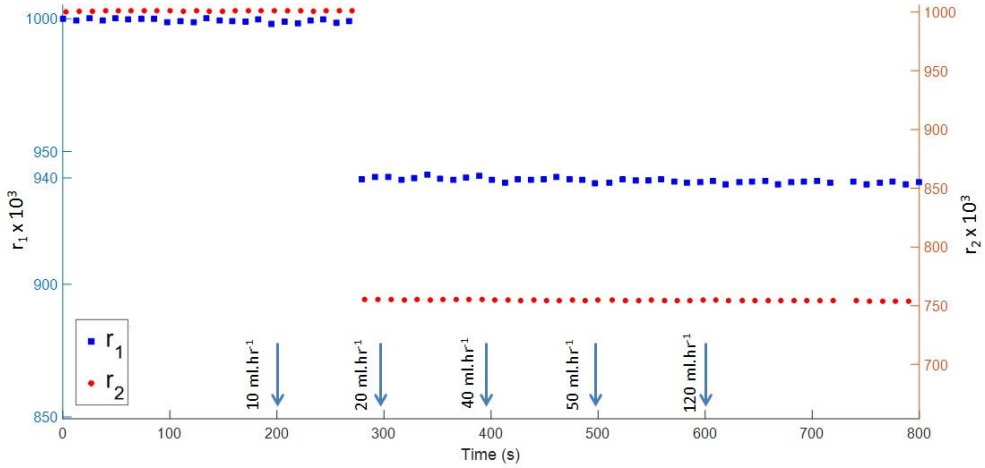

Figure 15 Variation of the acoustic reflection coefficients r_1 and r_2 with time for DTI 4 µm with 80 µ micro-channel using different flow rate of pure ethanol

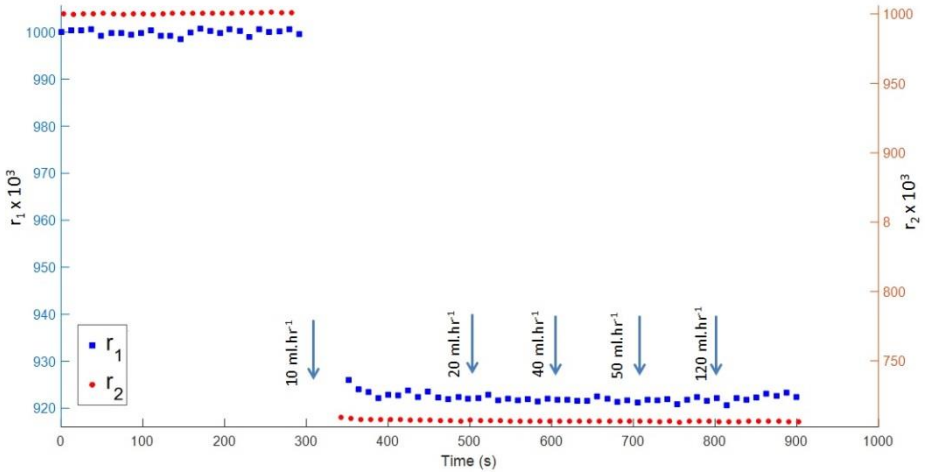

Figure 16 Variation of the acoustic reflection coefficients r_1 and r_2 with time for DTI 4 µm with 80 µ micro-channel using different flow rate of distilled water

The two flow rates (liquid speeds inside the micro-channel) measurements with DW and pure ethanol show that changing it from 10 ml.hr^{-1} to 120 ml.hr^{-1} has no effect on the wetting transition inside the trenches.

4. CONCLUSION

In this paper, characterization of the wetting behavior using the acoustic reflection coefficient is performed on four types of DTI wafer with different etches depth (4, 5, 6 and 7 µm). For the first time, we present the acoustic technique coupling with fluidic flow thanks to the use of PDMS based micro-channels. For each type of DTI sample two micro-channels with different thickness (40 and 80 µm) were used to inject the different liquids. The measurements with the 40 µm micro-channels were performed using different water / ethanol mixtures and we showed that for the four DTI wafers non-complete and partial wetting behavior were observed. With the 80 µm micro-channels, a new real-time technique was introduced for the assessment of the reflection coefficients on the top and bottom echoes. This technique enabled faster data acquisition time and also direct observation of the wetting and drying phases. The same measurements using water / ethanol mixtures were performed on the DTI wafers with 80

μm micro-channels and a similar behavior of partial wetting to the one observed using the 40 μm micro-channel was obtained on the four DTI wafers. Finally, using the 80 μm micro-channel, we did measurements with distilled water and pure ethanol using different flow rates on the DTI 4 μm with 80 μm micro-channel and we saw that there was no effect on the wetting state for the different flow rates (10 $ml.h^{-1}$ – 120 $ml.h^{-1}$).

In our different measurements, it seems that a partial wetting state is common among the different DTI sample. This partial state implies that the cleaning of the DTI will be incomplete which supports the problem faced at the microelectronic industry in cleaning high AR structures. In future study, we will examine the drying process of the different DTI samples as we will investigate the wetting transition phenomenon due to pressure changes and the deformation of the structures due to pattern collapse.

Acknowledgements

This work was partially supported by the French Renatech network. This research work has been partially undertaken with the support of IEMN fabrication (CMNF).

The authors would like to thank the Program NANO 2022 supporting the joint lab IEMN - STMicroelectronics.

REFERENCES

[1] Moore G.E., "Cramming more Components onto Integrated Circuits, *Reprinted from Electronics, Volume 38, Number 8, April 19, 1965, Pp.114 Ff.," IEEE Solid-State Circuits Society Newsletter 11(3), 33-35,(2006).*

[2] Kumar, S., "Fundamental Limits to Moore's Law," *ArXiv: Mesoscale and Nanoscale Physics*, (2015).

[3] W. Arden, M. Brillouët, P. Cogez, M. Graef, et al.," " More-than-Moore " White Paper," *The International Technology Roadmap for Semiconductor*, (2010).

[4] Xu, Xiumei & Vereecke, Guy & Hoogen, Erik & Smeers, Jens & Armini, Silvia & Delande, Tinne & Struyf, Herbert, "Wetting Challenges in Cleaning of High Aspect Ratio Nano-Structures," *Solid State Phenomena* 195, 235-238 (2012).

[5] A. B. D. Cassie, "Contact angles," *Discuss. Faraday Soc.* 3, 11-16 (1948).

[6] Kumar, Shashi & Saha, Tamoghna & Das, Ajit & Bhaumik, Soubhik., "LOTUS-LEAF EFFECT AND ITS APPLICATION IN DRAG REDUCTION," (2015).

[7] R. N. Wenzel, "Resistance of solid surfaces to wetting by water," *Ind. Eng. Chem.* 28(8), 988–994 (1936).

[8] A. Marmur, "Wetting on hydrophobic rough surfaces : to be heterogeneous or not to be?," *Langmuir* 19(20), 8343–8348 (2003).

[9] Peter, Daniel, "Pattern Collapse - the Mechanical Stability and Solid Bridging of Semiconductor Nanostructures," (2010).

[10] H. Namatsu, K. Kurihara, M. Nagase, K. Iwadate, and K. Murase, "Dimensional limitations of silicon nanolines resulting from pattern distortion due to surface tension of rinse water," *Appl. Phys. Lett.* 66(20), 2655–2657 (1995).

[11] Arnaud, Tournier & Leverd, F & Favennec, L & Perrot, C & Pinzelli, L. & Gatefait, M & Cherault, N & Jeanjean, Damien & Carrere, J.-P & Hirigoyen, F. & Grant, Lindsay, "Pixel-to-Pixel isolation by Deep Trench technology: Application to CMOS Image Sensor," (2011).

[12] Kung, Chun Haow (Bryan) & Sow, Pradeep & Zahiri, Beniamin & Mérida, Walter, "Assessment and Interpretation of Surface Wettability Based on Sessile Droplet Contact Angle Measurement: Challenges and Opportunities," *Advanced materials interfaces* 6(18), (2019).

[13] Vrancken, N., Li, J., Sergeant, S., Vereecke, G., Doumen, G., Holsteyns, F., Chen, C., Terryn, H., De Gendt, S., & Xu, X., "In-situ ATR-FTIR for dynamic analysis of superhydrophobic breakdown on nanostructured silicon surfaces," *Scientific Reports* 8(1), 11637 (2018).

[14] Virgilio, C. , Carlier, J. , Campistron, P. , Toubal, M. , Garnier, P. , Broussous, L. , Thomy, V. , Nongaillard, B., "Wetting Characterization of High Aspect Ratio Nanostructures by Gigahertz Acoustic Reflectometry," *International Journal of Mechanical and Mechatronics Engineering* 10(3), 506-511 (2016).

[15] Mallet, Antoine & Prat, Marc & Broussous, Lucile & Schmitz, Philippe, "Cleaning Process in Single Wafer Tool: Impact of Dispersion Phenomena on Rinsing Time," *ECS Transactions* 25, (2009).

[16] Christophe Virgilio, L. Broussous, P. Garnier, Julien Carlier, Pierre Campistron, et al., "Deep Trench Isolation and Through Silicon Via Wetting Characterization by High-Frequency Acoustic Reflectometry," *Solid State Phenomena* 255, 129-135 (2016).

[17] Mathieu Foucaud, "Etude de la dégradation de la protection par des résines photosensibles de la grille métallique TiN lors de gravures humides pour la réalisation de transistors de technologies sub-28nm," (2015).

[18] Bhatelia, T., Utikar, R., Pareek, V., & Tadé, M., "CHARACTERIZING LIQUID FILM THICKNESS IN SPINNING DISC REACTORS," (2009).

[19] D. Zamani, K. Dhane, O. Mahdavi, M. Anthony, J. Yan, and F. Shadman, "surface cleaning of small structures during spin rinsing of patterned substrates," *Microelectronic Engineering* 108, 57-65 (2013).

[20] Wehking, Jonathan, "Pressure Losses Experienced By Liquid Flow Through Pdms Microchannels With Abrupt Area Changes," (2008).

[21] Wang, Yunpeng and Khayat, Roger, "Impinging jet flow and hydraulic jump on a rotating disk," *Journal of Fluid Mechanics* 839, 525-560 (2018).

[22] Bhagat, Rajesh K., et al., "On the origin of the circular hydraulic jump in a thin liquid film," *Journal of Fluid Mechanics* 851, (2018).

[23] Cordoba, Jhonattan and Schianti, Juliana and Almeida, Maria and Pavani, Aristides and Panepucci, Roberto and Hernández Figueroa, Hugo Enrique and Gabrielli, Lucas, "Low-loss modified SU-8 waveguides by direct laser writing at 405 nm", *Optical Materials Express* 7, 2651 (2017).

[24] Golvari P, Kuebler SM., "Fabrication of Functional Microdevices in SU-8 by Multi-Photon Lithography," *Micromachines* 12(5), 472 (2021).

[25] E. Alvarea, G. Vazquez, and J. M. Navaza, "Surface tension of alcohol + water from 20 to 50 °C," *J. Chem. Eng. Data* 40(3), 611-614 (1995).

[26] Malviya, Abhigyan & Vrabec, Jadran, "Henry's Law Constant of Nitrogen, Oxygen, and Argon in Ternary Aqueous Alcoholic Solvent Mixtures," *Journal of Chemical & Engineering Data* 65(3), 1189-1196 (2019).

[27] Battino, Rubin & Rettich, Timothy & Tominaga, Toshihiro, "The Solubility of Nitrogen and Air in Liquids," *Journal of Physical and Chemical Reference Data* 13(2), 563-600 (1984).

[28] A. Guha and Debaprasad Panda, "Solubility of some non-polar gases in mixed solvants," *Int. J. Chem.* 6(3), 1147-1167 (2008).